The feasibility of pulse compression by nonlinear effective bandwidth extension

Gregory T. Clement[a)]
Department of Radiology, Harvard Medical School and Brigham & Women's Hospital, Boston, Massachusetts 02115

Hideyuki Nomura and Tomoo Kamakura
The University of Electro-Communications 1-5-1, Choufugaoka, Choufu-shi, Tokyo Japan 182-8585

(Received 24 October 2010; revised 25 July 2011; accepted 25 July 2011)

Chirp-encoded excitation has been utilized for increased signal-to-noise ratio (SNR) in both linear and harmonic imaging. In either case, it is necessary to isolate the relevant frequency band to avoid artifacts. In contrast, the present study isolates and then combines the fundamental and the higher harmonics, treating them as a single, extended bandwidth. Pulse-inverted sum and difference signals are first used to isolate even and odd harmonics. Matched filters specific to the source geometry and the transmit signal are then separately applied to each harmonic band. Verification experiments are performed using up to the third harmonic resulting from an underwater chirp excitation. Analysis of signal peaks after scattering from a series of steel and nylon wires indicates increased compression using the extended bandwidth, as compared to well-established methods for fundamental and second harmonic chirp compression. Using third harmonic bands, a mean pulse width of 56% relative to fundamental compression and 48% relative to second harmonic compression was observed. Further optimization of the compression by altering the transmission indicated 17% additional reduction in the pulse width and a 47% increase in peak-to-sidelobe ratio. Overall, results establish the feasibility of extended bandwidth signal compression for simultaneously increasing SNR and signal resolution. © *2011 Acoustical Society of America*. [DOI: 10.1121/1.3625236]

PACS number(s): 43.25.Cb, 43.80.Qf, 43.80.Vj, 43.60.Ek [OAS] Pages: 1810–1819

I. INTRODUCTION

Ultrasound coded excitation schemes[1] have become an established technique for enhancing signal-to-noise (SNR) ratios in ultrasound imaging.[2–4] Originating from signal compression techniques in radar,[5] a wide range of ultrasound-tailored approaches[1,6–11] have been developed. Accordingly, various medically motivated applications have been investigated[2,12–15] including its potential as a method for harmonic imaging with contrast bubbles.[2,16–18]

Regardless of specific technique, methods follow a common fundamental principle: to extend a signal in time, so that its total energy far exceeds that of an equivalent impulse.[19] Pulse compression, i.e., temporal localization, of the received signal is then achieved through matched filtering.[20] In practice, this operation adds complexity to an imaging system while increasing processing time, motivating the development of faster[6–8,21] and more optimized implementation.[12,22–24] Despite adding complexity, the approach can have particular advantage in medical applications, where limits pertaining to the pulse amplitude, e.g., spatial-peak peak-average intensity (I_{sppa}) and mechanical index can be substantially lowered while maintaining the same overall temporal average, e.g., spatial-peak temporal-average intensity (I_{spta}).[25]

Pulse compression for nonlinear signals has also been performed.[16,17,27] These nonlinear methods operate by isolating higher harmonic signal components, which are then filtered in a manner similar to linear pulse compression. Although still band-limited, the second harmonic generally offers increased radial focusing abilities and a potentially broader bandwidth relative to the fundamental. Unfortunately, such techniques can suffer artifacts caused by overlap between the harmonics.[27] Moreover, isolated use of the harmonic signal for compression can become degraded due to increased absorption as a function of frequency.[28]

The present work studies an alternative approach to nonlinear compression that combines the fundamental and higher harmonics, effectively treating them as a single band. This *extended bandwidth* permits a significant increase in the ability to compress a signal. Successfully implemented, the method would permit enhanced image resolution while benefiting from the increased SNR offered by encoding.

However, phase trends between the fundamental signal and the harmonics can differ substantially, making the design of an extended matched filter nontrivial. These potentially detrimental phase differences are the primary barrier to directly combining the harmonics. Generally, the phase relation between an initial pulse and the harmonics it generates is a function of input pressure, temporal and spatial beamshape, and aperture geometry.[29] Moreover, as energy from higher harmonics is continually transferred back into the fundamental frequencies, the fundamental's phase is also altered as a function of distance. Attempts to compress a signal by simple cross correlation could be limited, or even cause degradation, as compared to linear compression. Therefore, further modification of the signal is clearly necessary if the approach is to be affective.

[a)]Author to whom correspondence should be addressed. Electronic mail: gclement@hms.harvard.edu

The modification proposed here involves a multistage approach, originating from a signal that starts as a modified linear chirp transmission.[2] Using a standard pulse inversion technique, two signals—each an inverted version of the other—are transmitted in order to separate even and odd harmonics of the received signal. Phase analysis is used to form separate matching filters for the first, second, and higher harmonics. Specifically, acceleration of the signal phase angle is determined from the second derivative with respect to frequency of each signal's Fourier transform, whereas the first derivative provides information on any relative phase offset between the different harmonics. Matched filters are then formed from this analysis. In practice such filters could be designed *a priori*. In a final stage, the higher harmonics are amplified at the time of acquisition, based on a one-dimensional optimization of the signal.

The theoretical foundation for the method is outlined here, followed by experimental verification using underwater ultrasonic measurements. Compressed pulses are evaluated by comparison with signals formed by correlation of the fundamental and second harmonic signals, respectively. Optimization of transmission pulses is considered, as well as an assessment of the approach under noisy and attenuating conditions.

II. THEORY

A. Physical basis

The linear combination of two or more frequency-shifted, but otherwise equal frequency bands will result in a time domain signal whose modulation amplitude is identical to that of a single band. Thus, simply combining bands does not imply increased temporal localization. Compression beyond that of the modulation width, rather, requires cancellation between the carrier and modulating functions. This process can be illustrated analytically for the case of a boxcar function. The maximum time-domain compression—i.e., signal localization—about the origin occurs when the phase of the function's Fourier transform is a constant with respect to frequency.[2] In this case, integral components of the inverse transform will be in phase at time $t=0$. For a function defined in terms of constant amplitude P_0, center frequency ω_c, and bandwidth ω_b,

$$P_1(\omega) = \begin{cases} P_0, & \omega_c - \omega_b/2 \le \omega \le \omega_c + \omega_b/2 \\ 0, & \text{otherwise,} \end{cases} \tag{1}$$

the inverse Fourier transform (IFT) may be expressed in terms of a continuous-wave signal of frequency ω_c, modulated by an unnormalized sinc function,

$$p_1(t) = \mathrm{IFT}\{P_1(\omega)\} = P_0\omega_b e^{i\omega_c t}\mathrm{sinc}(\omega_b t/2). \tag{2}$$

The relevant case combines the fundamental and propagation-generated second harmonic, comprising two bands centered about ω_c and $2\omega_c$, and differing in amplitude by a factor σ. Ideally, the bandwidth of the second harmonic is twice the fundamental, but will generally be smaller due to frequency dependence of both the rate of nonlinear buildup and absorption. In an example case where bandwidths are equal, by Eq. (1) the total spectrum is $P(\omega)=P_1(\omega) + \sigma P_1(\omega-\omega_c)$. Using the shift property of Fourier transforms, it follows from Eq. (2) that the time-domain representation of this function is then given by

$$p(t) = P_0\omega_b e^{i\omega_c t}\mathrm{sinc}(\omega_b t/2)\left(1+\sigma e^{i\omega_c t}\right) \tag{3}$$

Noting that zero crossings of Eq. (3) due to the sinc term occur at nonzero even integers,

$$p(t) = 0; \qquad t = \frac{\pm n\pi}{\omega_b}, \qquad n = 2, 4, \ldots, \tag{4}$$

whereas minima of the modulus of the second bracketed term occur at odd integers:

$$p(t) = 0; \qquad t = \frac{\pm n\pi}{\omega_c}, \qquad n = 1, 3, \ldots; \tag{5}$$

when $\omega_c \sim \omega_b$ the sinc serves to suppress all extrema of the carrier, except at the origin. This results in reduced sidelobes and as $\sigma \Rightarrow 1$, a signal peak approximately equal to a single band with center frequency $3\omega_c/2$ and bandwidth $2\omega_c$. In the case where $\omega_c \gg \omega_b$, the signal envelope is equal to the modulus of the sinc function, and thus the signal width is determined by the modulation.

Similar behavior occurs for bands consisting of smooth functions. A Gaussian-shaped band will produce a Gaussian-shaded time domain signal, but two combined bands will contain periodic peaks. or two peaks defined by the envelopes $\exp[-(\omega-\omega_c)^2\, 4\sqrt{\ln 2}/\omega_b^2]$ and $\sigma\exp[-(\omega -2\omega_c)^2 4\sqrt{\ln 2}/\omega_b^2]$, such that their half-maxima are equal to ω_b, the inverse Fourier transform[30] gives

$$p(t) = \frac{\omega_b}{4}\sqrt{\frac{\pi}{\sqrt{\ln 2}}}\, e\left(-\omega_b^2 t^2/16\sqrt{\ln 2}\right) \times e(i\omega_c t)[1+\sigma\, e(i\omega_c t)]. \tag{6}$$

Once again the shift property has been utilized to combine the signals.

Defining a precise optimal bandwidth for waveforms is arbitrary, depending upon whether minimizing the beamwidth or sidelobes takes precedent, but will generally entail an optimization of the two. For illustration, the examples above use only two identical-width bands. Generalization to N bands and asymmetric bandwidths—although more cumbersome to express analytically—have related behavior. Figure 1 illustrates such an example by comparing two asymmetric narrow band cases resulting from a second harmonic $0.5\times$ the amplitude of the fundamental with both a relatively narrow band ($0.244\omega_c$), and a broader bandwidth (0.667).

Building on this basis, the goal of the extended bandwidth approach will be to produce a transmitted pulse that, upon the buildup of nonlinear harmonics will produce a bandwidth that can produce temporal localization exceeding that of a given single band. In Sec. IV, a range of relative bandwidths resulting from a chirp signal are considered. Additionally, the

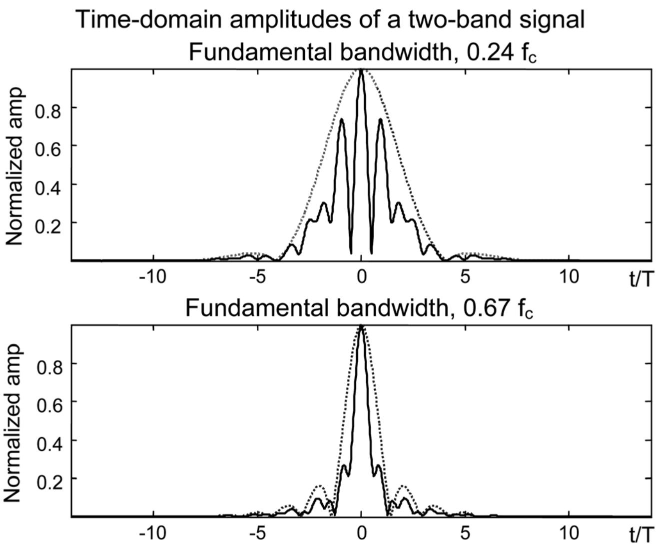

FIG. 1. Time-domain amplitudes of a two-band signal with a 24% (upper) and 67% (lower) bandwidth of center frequency f_c. The second band is 1/2 the amplitude and approximately 1.8 times wider and twice the center frequency of the fundamental. The dotted line shows the fundamental's time-domain amplitude for comparison.

effects of bandwidth shape is examined for a range of functions having relatively flat bandwidth but smooth cutoff, i.e., functions intermittently shaped between Eqs. (3) and (6).

B. Frequency domain representation

Generation of frequency bands for compression is based on the transmission of a linear chirp of duration T. In the time domain, the function can be represented by

$$p(t) = \begin{cases} p_0(t)\, e^{\left[i\left(\omega_0 t + (\alpha/2)t^2\right)\right]}, & 0 \le t \le T \\ 0, & \text{otherwise,} \end{cases} \qquad (7)$$

where $p_0(t)$ is a weighting function, α is the angular acceleration of the signal, and the instantaneous frequency is given $\omega = \omega_0$ at $t = 0$ and $\omega = \omega_0 + \alpha T$ at $t = \mathrm{T}$. Considering first the case where p_0 is time-independent, the Fourier transform of Eq. (7) can be written in the form

$$p(\omega) = p_0\, e\left[-i\frac{(\omega-\omega_0)^2}{2\alpha}\right] \int_0^T e\left[i\frac{\alpha}{2}\left(t - \frac{\omega-\omega_0}{\alpha}\right)^2\right] dt. \qquad (8)$$

Substituting so that $\sqrt{\alpha/2}\{t - (\omega-\omega_0)/\alpha\} = \sqrt{\pi/2}\,\xi$, so that

$$t = 0, \qquad \xi_0 = -\sqrt{\frac{\alpha}{\pi}}\frac{\omega-\omega_0}{\alpha},$$
$$t = 0, \qquad \xi_1 = \sqrt{\frac{\alpha}{\pi}}\left\{T + \frac{\omega-\omega_0}{\alpha}\right\}, \qquad (9)$$

a change of variables then allows Eq. (8) to be rewritten as

$$P(\omega) = p_0\, e\left[-i\frac{(\omega-\omega_0)^2}{2\alpha}\right] \sqrt{\frac{\pi}{\alpha}} \int_{\xi_0}^{\xi_1} e\left(i\frac{\pi}{2}\phi\xi^2\right) d\xi. \qquad (10)$$

In this form, the integral in Eq. (10) can be expressed in terms of the Fresnel integrals $C(x)$ and $S(x)$, defined by

$$C(x) + iS(x) = \int_0^x \exp\left(i\frac{\pi}{2}t^2\right) = \int_0^x \cos\left(\frac{\pi}{2}t^2\right)dt + i\int_0^x \sin\left(\frac{\pi}{2}t^2\right)dt. \qquad (11)$$

As the Fresnel integrals are odd functions, along with the integral limits in Eq. (9) they confine the phase of the integral in Eq. (10) to the first quadrant. The main contribution to phase change with frequency is therefore $\exp[-i(\omega-\omega_0)^2/\ 2\alpha]$ Further, if the first-quadrant phase fluctuations introduced by the Fresnel integrals are assumed to have a negligible net effect on compression, then optimal compression can then be achieved through multiplication by $\exp[-i(\omega-\omega_0)^2/2\alpha]$.

If nonlinear propagation is considered, however, the phase relation between the fundamental and harmonic frequencies must also be considered. In general, this phase is a function of transmission pressure, beam shape and aperture geometry, making it potentially difficult to predict. In a lossless medium, a received signal's mth harmonic band due to reflection at N locations can be written as

$$P_m(\omega) = P_{m_0}\, e\left[-i\frac{(\omega-\omega_{m_0})}{2\alpha_m}\right] e(-iT_m\omega) \sum_{n=1}^{N} q_{m,n} \times e\left(-i2\frac{Z_n}{c}\omega\right), \quad \omega_{m_0} \le \omega \le \omega_{m_1}, \qquad (12)$$

where T_m represents a temporal offset between the harmonics and $q_{m,n}$ are the scattering strengths of the mth harmonic signal. An example of such a signal is provided in Fig. 2, using data collected per the experimental arrangement described in Sec. II A. Waves are assumed to propagate linearly after scattering. In a weakly nonlinear case α_1 is approximately equal to the angular acceleration of the transmitted signal α. However α_1, and its higher harmonic equivalents are currently regarded as constants of the equation, to be determined.

A received time-domain signal $p_+(t) = p_1(t) + p_2(t)$, and its corresponding pulse-inverted signal $p_-(t) = -p_1(t) + p_2(t)$ can be separated by, respectively, taking 1/2 of the addition and subtraction of the two signals. Provided that the even and odd Fourier transformed bandwidths are sufficiently spaced to separate the mth and mth$+2$ bands, then Eq. (12) may be approximated. The transforms may be arranged in a form recognized as series of pure imaginary linear equations,

$$\mathrm{Im}\left\{\frac{1}{P_m}\frac{dP_m}{d\omega}\right\} = \left(-\frac{1}{\alpha_m}\right)\omega + \left(\frac{\omega_0}{\alpha_m} - 2\frac{z}{c} - T_m\right), \qquad (13)$$

where the parenthetical terms on the right-hand side of Eq. (13) give slope and intercept values, respectively. Solving for these values by linear regression, and combining equations to eliminate z/c allows a matched filter for Eq. (12) to be written as

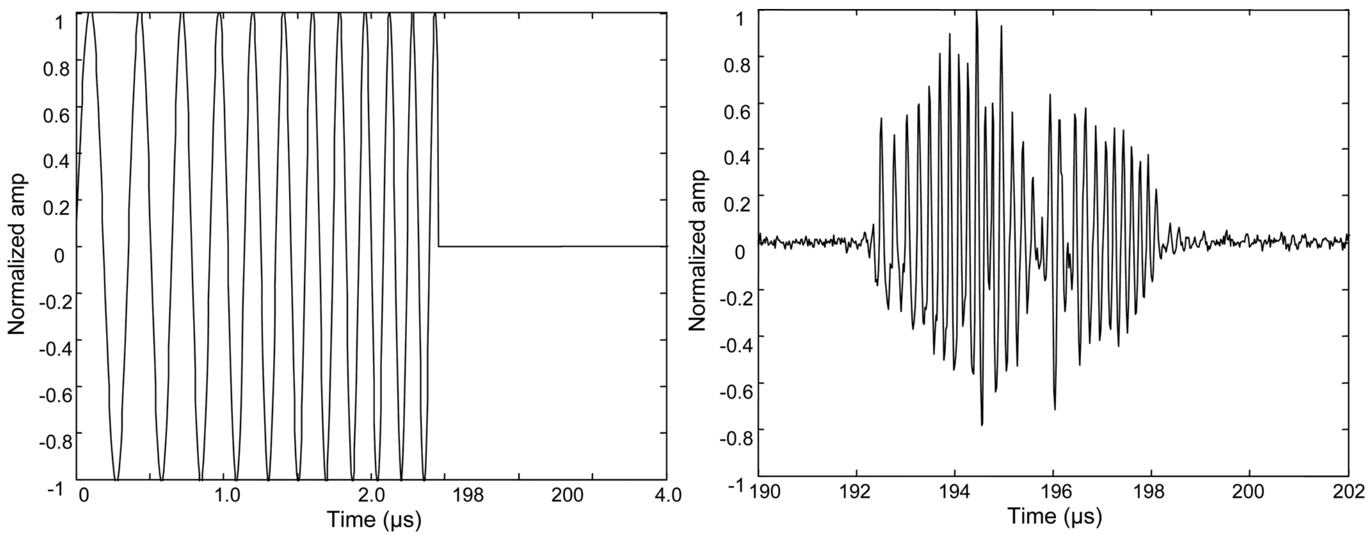

FIG. 2. Overlapping chirp signals due to scattering from three objects. The second and third objects are 0.5 and 5 mm, respectively, from the first.

$$\tilde{P}_m(\omega) = e\left[i\frac{(\omega-\omega_{m0})^2}{2\alpha_m}\right]e(iT_m\omega). \quad (14)$$

In theory these matching filters could be determined, or at least approximated, by a calibration procedure for a given array and application. The overall process is illustrated in Fig. 3 using scattering data described in detail in the next section. Figure 3 shows the Fourier transformed amplitude of an example signal plus/minus its inversion. This transformed signal is processed according to the left-hand side of Eq. (13), before (center) and after (bottom) the application of Eq. (14).

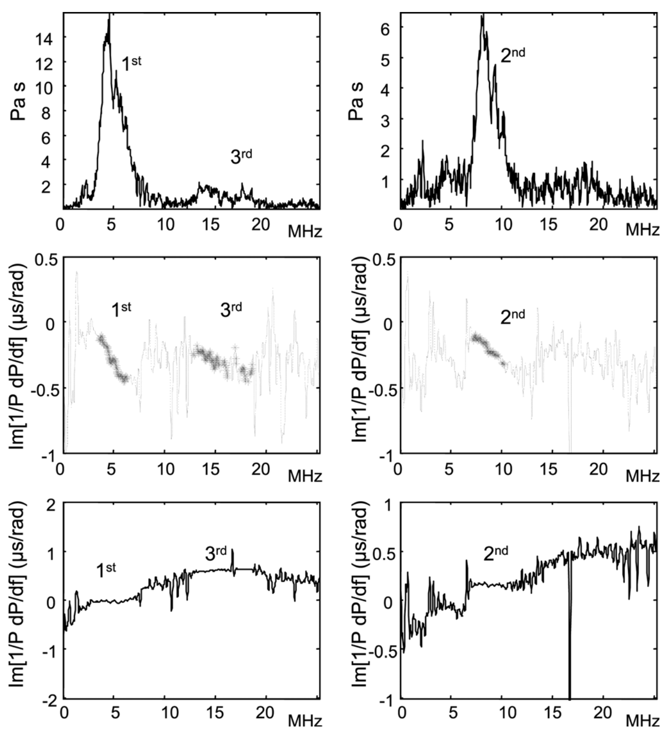

FIG. 3. (Top) Amplitude of the Fourier transformed signal consisting of odd harmonics acquired by summation of a signal and its inversion (left) and even harmonics produced from the signal differences (right). (Middle) Derivative of phase with respect to frequency for the odd harmonic (left) and even harmonic (right). (Bottom) Derivative of phase with respect to frequency after application of a weighting factor to remove quadratic terms.

Once phase matched, further compression of the signal is possible through amplification of individual bands. The optimal extent of amplification is specific to the signal, so that this process is suitable for application after acquisition. As time-separated reflections appear as interference peaks in the frequency domain, direct normalization of the signal would remove this information. Hence, an amplitude filter consisting of a uniform elevation of each harmonic is applied. Presently, the optimum value of the increase is determined through a 1D optimization that minimizes the ratio between first local maxima and the signal peak of a successively larger number of harmonics. Initially, only the first and second harmonic signals are combined,

$$\tilde{p}_{\mathrm{opt}}(t) = \mathrm{IFT}\{P_1(\omega)\tilde{P}_1(\omega) + N_2P_2(\omega)\tilde{P}_2(\omega)\}, \quad (15)$$

where the resultant signals is evaluated over a specified range, N_2, and noting that the functions of P_1 and P_2 may overlap. This adjusted signal can then be used to select the amplification for the third harmonic

$$\tilde{P}_{\mathrm{opt}}(t) = \mathrm{IFT}\{P_1(\omega)\tilde{P}_1(\omega) + N_2P_2(\omega)\tilde{P}_2(\omega) + N_3P_3(\omega)\tilde{P}_3(\omega)\}. \quad (16)$$

In theory, the process can be repeated for an arbitrary number of harmonics, but has been verified experimentally in the following up to three harmonics (Sec. IV).

III. MATERIALS AND METHODS

A. Verification

An initial underwater ultrasound experiment was devised to test the approach using the first three harmonics of a signal scattered from small objects. The goal of this experiment was to verify that data acquired experimentally could be compressed in the manner predicted by theory and a preliminary simulation study,[31] as well as to quantify differences between the proposed and existing compression methods.

A 13 mm diameter, 5 MHz center-frequency circular planar transducer (Sonix, Inc., Type IS0513L) was selected as a transmitter. The input signal was a linear chirp with parameters similar to a prior simulation study,[31] approximating Eq. (7) with p_0 constant.

Transducer bandwidth was determined by impulse response measurement. Based on this measurement, a 2.46 μs time sweep was generated using $\omega_0 = 2\pi \times 3.4$ MHz and $\omega_1 = 2\pi \times 6.4$ MHz. Fresnel integrals given in Eq. (11) were calculated to generate phase fluctuations of less than $\pm 12°$ from the mean phase in this configuration. These signals were uploaded through a GPIB interface to an arbitrary waveform generator (NF Electronic Instruments, model 1940, Yokohama, Japan) and amplified by a power amplifier (Kalmus, model 150c, Bothell, WA). Success of the compression scheme was evaluated under the conditions of overlapping signals caused by scattering from thin wires. Two types of wire, 0.17 mm diameter nylon ($c = 2.6 \times 10^3$ m/s, $\rho = 1.1 \times 10^3$ kg/m^3) and 0.1 mm diameter steel ($c = 5.8 \times 10^3$ m/s, $\rho = 7.9 \times 10^3$ kg/m^3), were investigated separately. As illustrated in the upper frame of Fig. 4, three steel wires or three nylon wires were aligned within the path of a directed ultrasound field, such that the wires were extended at normal angles through the field's axis of propagation.

An 8 mm diameter focused transducer with a 12 mm radius of curvature (Custom build, SN: PT40-8-12, Toray Engineering Co.) was selected as a receiver based on its wide bandwidth, which ranged from below the transmitted bandwidth range to above the measurement cutoff frequency of 20 MHz. Received signals were sent through a low-pass filter set at 20 MHz and amplified (Panametrics, model 5073PR, Waltham, MA) before being recorded by a digital oscilloscope (LeCroy, model 6051, Chestnut Ridge, NY) at an 8-bit vertical resolution.

Due to the small sensitivity range of the receiver, backscatter measurements could not be performed without the receiver blocking the transmitted wave. Thus, an alternative experimental configuration was devised with the receiver's axis of symmetry situated perpendicular to the transmission field, the two axes intersecting in the region of the wires. The receiver was adjusted with the aid of a positioning stage, such that the wires were situated approximately within the same surface of constant receiving phase, and at a distance where the sensitivity was relatively flat across the 5 mm distance between the outermost wires. In this way, the times-of-flight between each wire and the transducer were approximately equal, allowing time delays to be equated to the distance between wires. The received signal was processed and evaluated for (i) the ability to maintain compression in the presence overlapping signals, (ii) the ability to differentiate between scattering locations, and (iii) for the accuracy of the reconstructed scattering locations. In all experiments, two wires were situated 5.0 mm apart. A third wire was placed between the two, at distances of 0.5, 1.0, 2.0, and 3.0 mm from the wire closest to the transmitter.

Data were acquired in four separate experiments. Two were conducted in the near-field, including 0.17 mm diameter nylon wire placed from $z_1 = 143$ mm from the transducer and 0.1 mm diameter steel wire placed from $z_1 = 192$ mm from the transducer. Far-field measurements for both the nylon and steel wire were conducted starting from $z_1 = 252$ mm from the transducer.

In an additional measurement set, the SNR was also investigated as a function of input amplitude. The SNR, as defined by the ratio of the mean signal to the standard deviation of the noise, was determined for both the raw and processed signals over this range. The signal was taken to be the period initially defined over a clearly defined (low-noise) pulse, and the SNR was calculated over all other points. In these measurements the center wire was fixed 1 mm from the first, whereas the voltage input to the power amplifier was varied between 5 and 400 mV, with regular 10 mV intervals below 50 mV (plus a measurement at 5 mV) and with 50 mV intervals up to 400 mV.

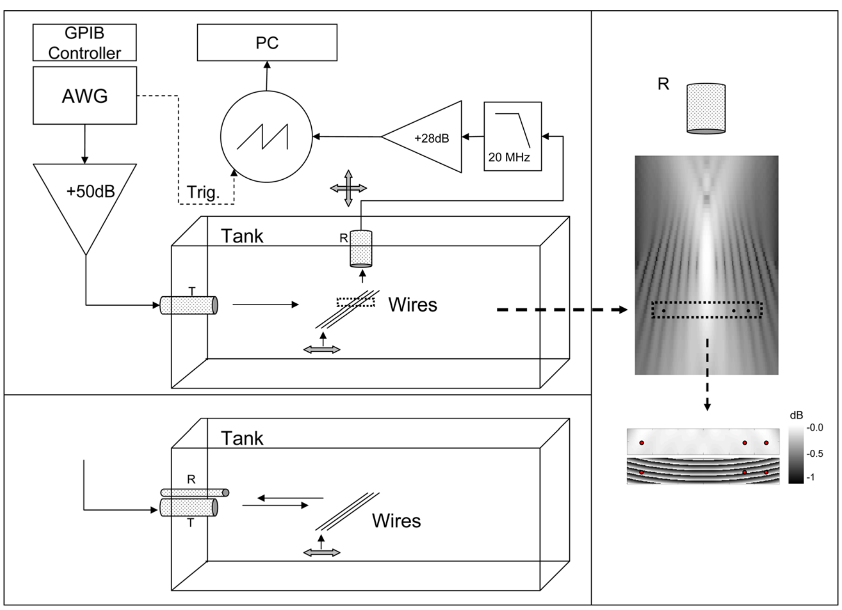

FIG. 4. (Color online) The experimental setup configured for (upper) normal scattering and (lower) backscattering.

B. Calibration

Prior to processing, the signal from a single wire was used to calculate the matched filters given by Eq. (14). Numeric values for the slope and intercept were determined over the frequency ranges where the first or second harmonic was most prominent. This range was arbitrarily selected as 40% of the signal peak. A least squares approach was used to fit the data, providing the slope and intercept values.

The slopes were observed to be approximately linear in the frequency bands where the signal amplitude is highest, indicating the phase approximates a second-degree polynomial, and validating the assumptions of the development of Eq. (14), at least for the present case. The substantial slope difference between the harmonics is also noted ($\alpha_1 = 1.49 \times 10^{13}\,\mathrm{rad/s^2}$, $\alpha_2 = 2.91 \times 10^{13}\,\mathrm{rad/s^2}$, $\alpha_3 = 6.07 \times 10^{13}\,\mathrm{rad/s^2}$) as this behavior is the primary motivation of the present work.

C. Pulse optimization

Based on verification results (detailed in the next section) a second study was devised to investigate the optimal weighting function $p_0(t)$ for the transmitted signal (7) using the first and second harmonics. Simulated waveforms were defined in the frequency domain over a specified bandwidth with cutoff frequencies smoothed by a Butterworth filter.[7,21] The slope of the cutoff, the bandwidth, and the relative amplitude difference between the fundamental and second harmonic bands were separately considered as independent variables. The cutoff slope was varied by changing the order n of the filter between $n = 1$, and $n = 20$. As the Butterworth response gain is monotonically decreasing, it produces no ripples and at lower orders resembles a slightly flattened Gaussian-like signal. At higher orders the cutoff becomes sharper and approximates a square-wave-like signal. Bandwidth was varied from 10% to 120% of the fundamental center frequency. The second harmonic peak amplitude was varied between 10% and 100% of the fundamental.

Dependency on the bandwidth of the second harmonic relative to the fundamental was also considered. In an idealized situation, the fundamental would produce a second harmonic bandwidth twice the fundamental. However, as the rate of increase of nonlinear-induced harmonics grows with the square of the frequency, and as higher harmonics are generally subject to measurably higher attenuation than the fundamental, the optimization was also performed with a band pass filter applied to the second harmonic.

Using the fundamental band as a control for the extended bandwidth compression, and using the first and second harmonics, it was observed that the minimum full-width-at-half-maximum (FWHM) as a percentage of the control was inversely proportional to bandwidth, whereas minimization of the peaks occurred in the region $\omega_c \sim \omega_b$ (Fig. 5), with the precise minimum dependent upon the relative amplitude of the second harmonic and the order number of the filter. Based on the criteria of (i) minimizing secondary peaks and (ii) minimizing the FWHM of the main peak, a filter of order $n = 10$ was selected, representing the intermittent range between a Gauss-like signal ($n = 1$), which optimized the former criterion, and a square-wave-like signal ($n \geq 20$), which optimized the latter. For the case of underwater nearly elastic scattering—i.e., the configuration being tested here—a 66% bandwidth was selected. Filtering of the two harmonic bandwidths—i.e., bandwidths that might be expected in a more attenuating environment—resulted in further minimization of sidelobes, but a reduced difference in the FWHM, compared to a single band's signal. In such cases, transmission bandwidths near 100% were found to be nearly optimal.

The 0.1 mm diameter three wire phantom was again used to evaluate the signals, but with a transducer (25 mm

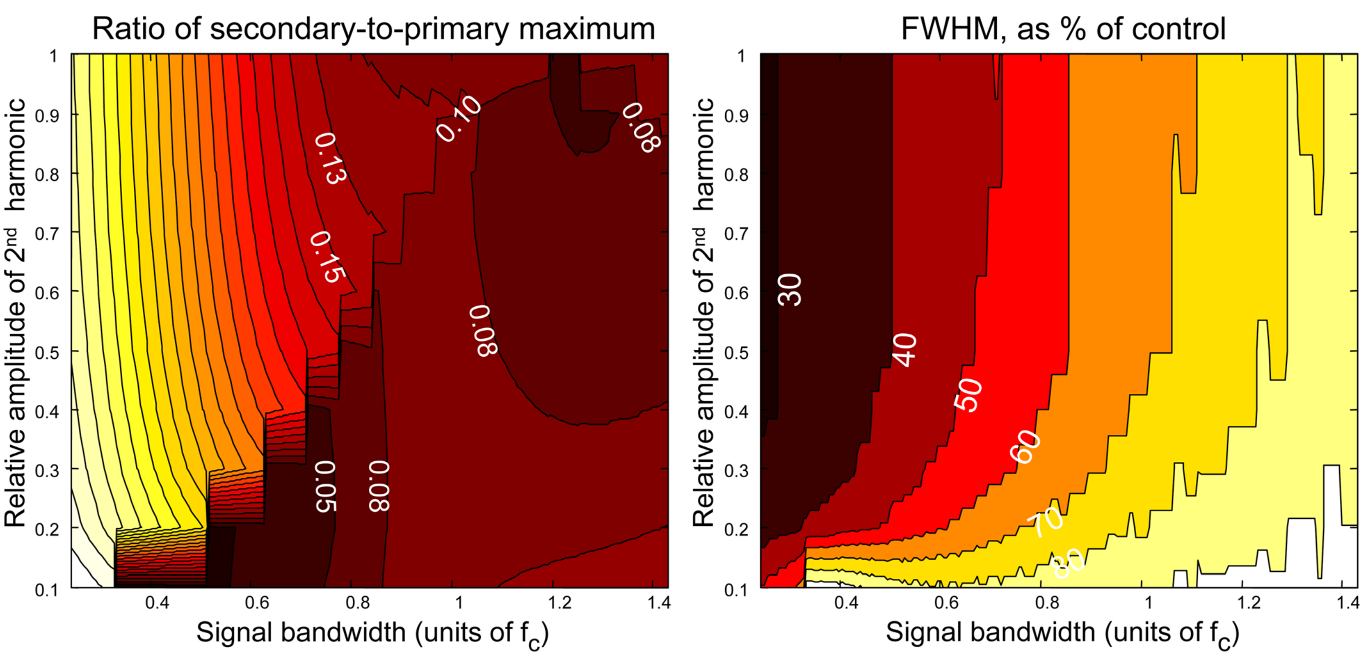

FIG. 5. (Color online) Simulation results for (left) minimization of the secondary peaks, shown for the case when the second harmonic bandwidth is twice the first. (right) Minimization of the FWHM for the same case.

diameter, f-number 4, $\omega_c = 2\pi \times 2.25$ MHz, Type A304s, Panametrics, Waltham, MA) and receiver (6.4 mm diameter, planar, $\omega_c = 2\pi \times 5.0$ MHz, Type A310S, Panametrics, Waltham, MA) affixed in a backscattering configuration (Fig. 4). Although the receiving transducer's bandwith was limited compared to the broadband receiver used in side scattering, the configuration allowed measurement in a configuration more likely to be encountered in medical and other diagnostic use. A pulser receiver was used to produce reference pulses (JSR DPR 35, JSR-Imaginant, Pittsford, NY). All other apparatus were identical to the experimental setup described previously. Processing was performed with the algorithm used in previous experiments.

Six transmission signals were tested (Fig. 6): Two stepped linear chirps P_{Chirp} ($\omega_0 = 2\pi \times 1.67$ MHz and $\omega_1 = 2\pi \times 3.33$ MHz at 66% and $\omega = 2\pi \times 1.25$ MHz and $\omega_1 = 2\pi \times 3.75$ MHz 100% bandwidth), two modified chirps P_M determined by the optimization (66% and 100% bandwidth), and two modified chirps that were further corrected P_{CM} using the modulus of the source-receiver-paired impulse response P_{ir},[19]

$$P_{\mathrm{CM}}(\omega) = P_M / |P_{ir}|. \quad (17)$$

The impulse response was determined from an impulsive signal using the aforementioned Panametrics pulser receiver (< 10 ns) reflected from a planar steel target.

IV. RESULTS

A. Verification

Upon compression, the received waveform was compared with compressed fundamental and second harmonic signals. The FWHM size, position, and variation in peak intensity were recorded for each case. When the center wire was greater than 1 mm from the first wire, three peaks were clearly distinguishable in all compression schemes. At 1 mm separation three distinguishable peaks were evident in all methods except the first harmonic compression, where the first two peaks were partially overlapping. Figure 7 shows an example of the compressed, received waveform consisting of the 0.17 mm diameter nylon with the center wire 1 mm from the first. The compressed first harmonic, second harmonic, extended signal using the first + second harmonics, and extended signal using the first + second + third harmonics are shown. Figure 8 shows a similar plot, but with the center wire now moved to 0.5 mm from the first. At this distance, only the extended bandwidth signals were able to resolve the first two objects. Similar behavior was observed in three of the four measurement configurations studied. In one case (0.1 mm wire in the far field), partially overlapping signals were still visible for the first harmonic and second harmonic compression. Cumulative results, including all positions of the center wire are summarized in Table I. Results indicate a reduced FWHM in all cases compared to first harmonic and second harmonic compression.

In measurements using the 0.17 mm wire, a substantial reduction in the third wire's signal amplitude was observed. This reduction is believed to result from receiver positioning. Although care was taken to align the detector, the assumption that the wires are equidistant from its surface is an approximation. Integration of the scattered signal over the surface of the receiver is believed to be a significant cause of the variation observed in signal amplitude. This variation may also be due, in part, to the directionality of scattering from the relatively thick 0.17 mm wires. This variation is detectable in the uncompressed as well as compressed signals, and there is a strong bias between variation of the first and second harmonic signals.

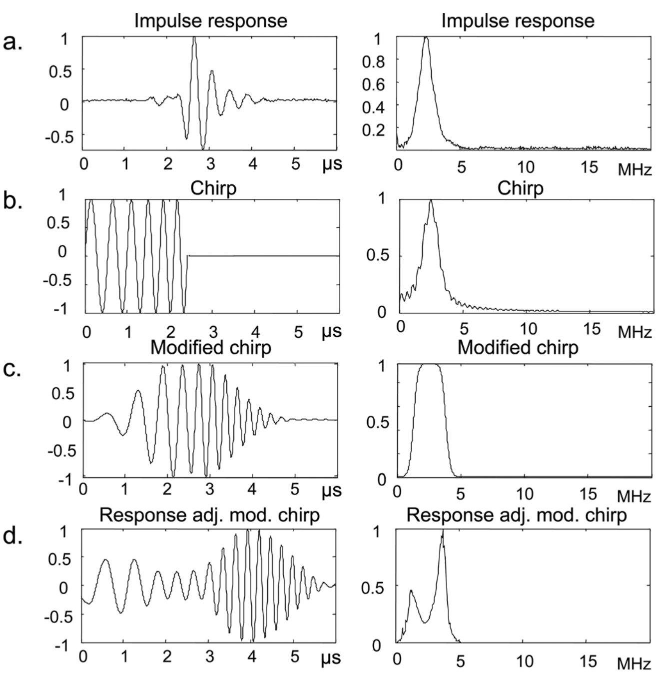

FIG. 6. (a) Impulse response of the transducer used for backscatter measurements. A linear chirp (b) is compared with a modified shaded chirp (c) created in the frequency domain and (d) a shaded chirp further modified to compensate for the transducer response. Waveforms here are for the 100% bandwidth case.

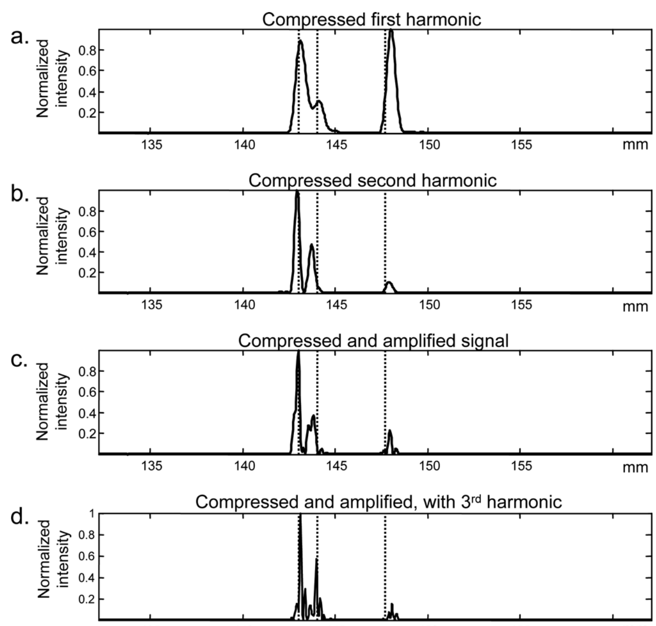

FIG. 7. Compressed signals scattered from three wires, when the second and wires are situated 1 and 5 mm from the first, respectively. Standard first (a) and second (b) harmonic compression are compared with the extended and amplified signals using two harmonics (c) and three harmonics (d).

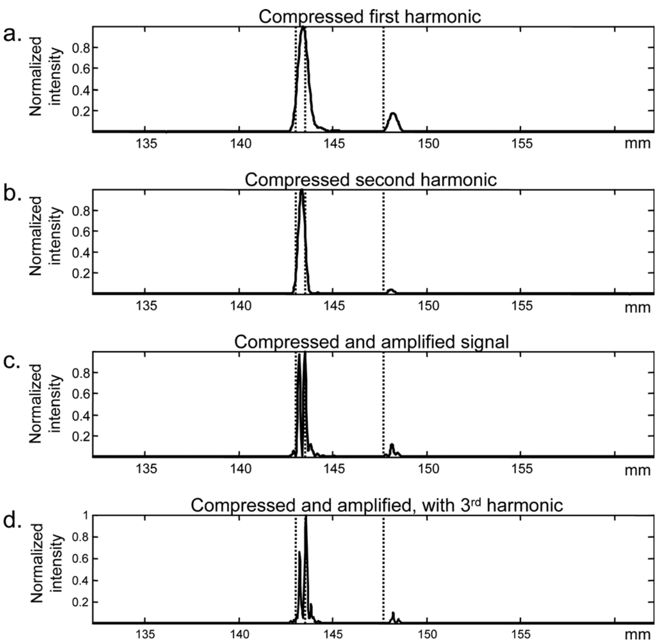

FIG. 8. Compressed signals scattered from three wires, when the second and third wires are situated 1 and 5 mm from the first respectively. Standard first (a) and second (b) harmonic compression are compared with the extended and amplified signals using two harmonics (c) and three harmonics (d).

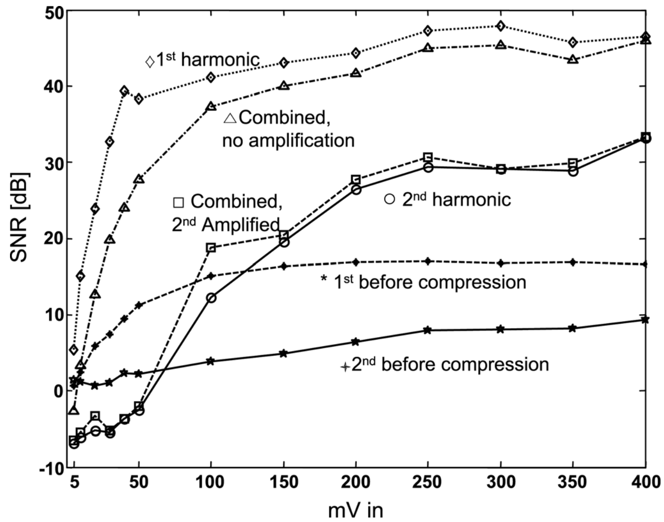

FIG. 9. The extension method's SNR (squares) closely follows that of the second harmonic signal (circles), and is significantly lower than when the amplification step is omitted (triangles). SNR of the first harmonic compression (diamonds) is appreciable even when the pre-compression SNR approaches 0 dB.

B. SNR

It was observed that the SNR of the compressed and amplified signal was closely dependent upon the SNR of the second harmonic. At lower amplitudes the ultrasound field was nearly linear and thus the second harmonic signal's SNR fell below 0 dB (Fig. 9).

The SNR was significantly improved when the extended bandwidth method was used, but without amplification. It was apparent from this result that amplification of the second harmonic also resulted in amplification of signal noise. These differences between the amplified and unamplified signals were particularly evident when the second harmonic signal was low.

At all voltage inputs, the resulting compressed first harmonic was clearly detectable. As indicated in Fig. 9, a first harmonic signal of significant amplitude was reconstructed, even when the raw signal's SNR was approaching the noise level ($V_{\text{in}} = 5$ mV, SNR first = 5.4 dB, SNR raw signals = 0.66 and 1.5 dB).

C. Pulse optimization

Modified chirp signals formed in the frequency domain were found to decrease the FWHM and increase the maximum peak-to-sidelobe ratio compared to the uncorrected chirp signal. Additional correction for the transducer's impulse response further improved both parameters. The net effects of this improvement are evident in the signal's compressed waveform shown in Fig. 10.

TABLE I. Summary of FWHM measurements using first harmonic compression, second harmonic compression, extended bandwidth compression with two harmonics, extended bandwidth compression with two harmonics plus uplifting (amplification) of the second harmonic, and extended bandwidth compression with three harmonics plus uplifting of the second and third harmonics.

0.1 mm diameter steel, $z = 192$ mm	Mean FWHM (mm)	±Δ (mm)	0.1 mm diameter Steel, $z = 252$ mm	Mean FWHM (mm)	±Δ (mm)
First harmonic	0.905	0.42	First harmonic	0.876	0.28
Second harmonic	0.887	0.49	Second harmonic	0.822	0.30
First and second extended	0.531	0.29	First and second extended	0.609	0.26
First and second extended, uplifting	0.434	0.29	First and second extended, uplifting	0.493	0.21
First, second, and third extended, uplifting	0.367	0.25	First, second, and third extended, uplifting	0.360	0.13

0.17 mm diameter Nylon, $z = 143$ mm	Mean FWHM (mm)	± Δ (mm)	0.17 mm diameter Nylon, $z = 252$ mm	Mean FWHM (mm)	± Δ (mm)
First harmonic	0.975	0.55	First harmonic	0.981	0.34
Second harmonic	0.631	0.56	Second harmonic	0.779	0.32
First and second extended	0.776	0.31	First and second extended	0.682	0.17
First and second extended, uplifting	0.585	0.29	First and second extended, uplifting	0.393	0.22
First, second, and third extended, uplifting	0.472	0.20	First, second, and third extended, uplifting	0.430	0.26

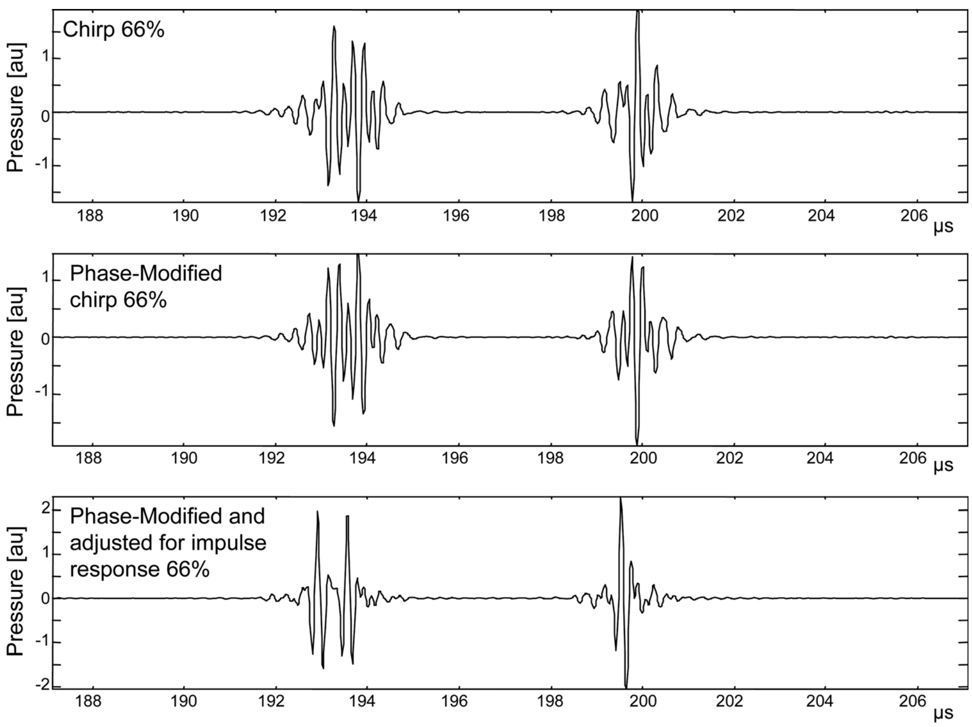

FIG. 10. Compressed echoes from three 0.1 mm wires placed 0.5 and 5 mm from the first. Chirp input signals (top) modified in the frequency domain (middle) increased compression, particularly when the transducer's response was accounted for (bottom).

Using a 66% bandwidth, the mean compressed FWHM was 0.51 mm for the chirp, 0.48 mm for the modified chirp, and 0.42 mm for the modified and corrected chirp. The peak-to-sidelobe ratio was 3.2 for the chirp, and 6.1 for both the modified chirp, and the modified and corrected chirp.

Compared to the 66% bandwidth, the 100% bandwidth was observed to be less than optimal, as predicted for the present low-attenuation conditions. The mean FWHM measurements yielded the following: chirp, 0.46 mm; modified chirp 0.49 mm; modified and corrected, 0.41 mm. The peak-to-sidelobe ratios were chirp, 4.6; modified chirp 5.1; modified and corrected, 5.3.

V. DISCUSSION

The primary benefit of pulse compression is the substantial increase in total energy that a transmitted signal can contain, and at the same time not exceeding the transmission capabilities of a given transducer, and without exceeding potential regulatory limits on ultrasound intensity or mechanical index. A wide range of medical, testing, and underwater applications can, and do, benefit from such techniques.

The present work has proposed a method for further compressing a signal by simultaneously utilizing its fundamental signal and the second harmonic generated from second order nonlinear propagation. In previous investigations the fundamental and the second harmonic have been separately utilized and the presence of more than one harmonic component has generally been treated as a source of artifacts.

In contrast, the extended bandwidth approach combines harmonics. Although combining bands does not automatically imply enhanced compression, proper choice of transmission bandwidth can result in cancellation between the signal envelope (or envelopes) and the secondary peaks of the carrier signal. The key to successful implementation is the quantification and subsequent correction of phase differences in each band. This correction is performed by phase analysis of a reference signal performed *a priori*. The resulting weighting factor provides a modified frequency domain signal, which resembles that of a compressed and propagated pulse whose bandwidth is extended relative to the transmission signal.

Signals can be further compressed by adjusting the relative amplitude of the higher harmonics, as applied *in situ*. Although other approaches may prove more robust, the present algorithm selected an amplification factor based on minimizing the total number of peaks in the signal. Using this method under nearly linear conditions and in the presence of noise indicated the benefits of the amplification step are diminished for noisy or small harmonics.

The approach was tested using three scattering sources; two overlapping and one reference. Working under low noise conditions, significant reduction in signal FWHM was observed, as compared to standard linear and second harmonic coded excitation. For the extended bandwidth approach, relative to first harmonic pulse compression (mean: 0.934 ± 0.40 mm), cumulative results of four experimental configurations found a 49% overall mean reduction in pulse width when using two combined harmonic bands (mean: 0.476 ± 0.25 mm) and 56% when using three harmonics (mean: 0.409 ± 0.24 mm). Relative to second harmonic pulse compression (mean: 0.780 ± 0.42 mm), reductions of 39% using two harmonics and 48% using three harmonics were observed.

Provided that there is sufficient signal strength, the approach expected to be applicable to an arbitrary number of harmonics. Practical application would likely require a specialized array, as well as a data acquisition scheme capable of a sampling rate sufficient to acquire multiple channels up to the desired harmonic band. Moreover, dedicated separate transmitted and received elements are likely, in order to optimize the output elements for power, and the received elements for bandwidth. Although not studied here, the ability to distinguish signal from artifact using a large dynamic imaging range could also prove to be a limit on certain applications. The present study was limited to the case of strong scatters.

A three-harmonic case was demonstrated here, showing enhanced waveform compression despite the third harmonic's relatively low amplitude. Although limited by the present experimental setup, this preliminary result motivates further investigation into ultraharmonic compression. Although not necessarily relevant to medical use, other potential applications (e.g., air-coupled ultrasound) may benefit from such work.

Examination of driving signals for the approach predicts that the precise optimal transmission signal will depend on the attenuation of the transmission and the strength of the nonlinearity. However, even if these values cannot be estimated with high precision, a sizable region exists (Fig. 5), where use of the extended bandwidth approach would still improve compression. Presently, optimal transmission bandwidths ranging between 66% and 120% were recorded for the various parameters studied here. For most cases no improvement or signal degradation was observed for bandwidths greater than 100%, indicating that, for the present approach, the maxim that more bandwidth is better does not apply.

VI. CONCLUSION

Coded excitation is commonly performed with the idea of increasing SNR at the expense of temporal (axial) resolution. However, the extended bandwidth method presented here has the potential to both increase SNR and also increase resolution relative to use the fundamental or second harmonic alone. In this preliminary study the method was found to have superior compression compared with coded excitation about the fundamental bandwidth, as well as second harmonic coded excitation. Future work will concentrate on experimental verification as well as improved methods for optimizing parameters in the matching filter.

ACKNOWLEDGMENT

G.T.C. was supported by the Japan Society for the Promotion of Science (JSPS) Invitational Fellowship Program, Award No. L10531.

[1]M. O'Donnell, "Coded excitation system for improving the penetration of real-time phased-array imaging systems," IEEE Trans. Ultrason. Ferroelectr. Freq. Control **39**, 341–351 (1992).

[2]T. Misaridis and J. A. Jensen, "Use of modulated excitation signals in medical ultrasound. Part I: Basic concepts and expected benefits," IEEE Trans. Ultrason. Ferroelectr. Freq. Control **52**, 177–191 (2005).

[3]T. X. Misaridis, K. Gammelmark, C. H. Jørgensen, N. Lindberg, A. H. Thomsen, M. H. Pedersen, and J. A. Jensen, "Potential of coded excitation in medical ultrasound imaging," Ultrasonics **38**, 183–189 (2000).

[4]M. H. Pedersen, T. X. Misaridis, and J. A. Jensen, "Clinical evaluation of chirp-coded excitation in medical ultrasound," Ultrasound Med. Biol. **29**, 895–905 (2003).

[5]C. Cook and J. Paolillo, "A pulse compression predistortion function for efficient sidelobe reduction in a high-power radar," Proc. IEEE **52**, 377–389 (1964).

[6]M. J. Bennett, S. McLaughlin, T. Anderson, and N. McDicken, "The use of the fractional Fourier transform with coded excitation in ultrasound imaging," IEEE Trans. Biomed. Eng. **53**, 754–756 (2006).

[7]J. Shen and E. S. Ebbini, "Filter-based coded-excitation system for high-speed ultrasonic imaging," IEEE Trans. Med. Imaging **17**, 923–934 (1998).

[8]M. Arif, D. M. J. Cowell, and S. Freear, "Pulse compression of harmonic chirp signals using the fractional Fourier transform," Ultrasound Med. Biol. **36**, 949–956 (2010).

[9]Y. Wang, K. Metzger, D. N. Stephens, G. Williams, S. Brownlie, and M. O'Donnell, "Coded excitation with spectrum inversion (CEXSI) for ultrasound array imaging," IEEE Trans. Ultrason. Ferroelectr. Freq. Control **50**, 805–823 (2003).

[10]R. Y. Chiao and X. Hao, "Coded excitation for diagnostic ultrasound: a system developer's perspective," IEEE Trans. Ultrason. Ferroelectr. Freq. Control **52**, 160–170 (2005).

[11]J. R. Sanchez, D. Pocci, and M. L. Oelze, "A novel coded excitation scheme to improve spatial and contrast resolution of quantitative ultrasound imaging," IEEE Trans. Ultrason. Ferroelectr. Freq. Control **56**, 2111–2123 (2009).

[12]S. Huang and P. Li, "Arbitrary waveform coded excitation using bipolar square wave pulsers in medical ultrasound," IEEE Trans. Ultrason. Ferroelectr. Freq. Control **53**, 106–116 (2006).

[13]M. O'Donnell and Y. Wang, "Coded excitation for synthetic aperture ultrasound imaging," IEEE Trans. Ultrason. Ferroelectr. Freq. Control **52**, 171–176 (2005).

[14]C. Hu, R. Liu, Q. Zhou, J. Yen, and K. K. Shung, "Coded excitation using biphase-coded pulse with mismatched filters for high-frequency ultrasound imaging," Ultrasonics **44**, 330–336 (2006).

[15]J. Cowe, J. Gittins, and D. H. Evans, "Coded excitation in TCD ultrasound systems to improve axial resolution," Ultrasound Med. Biol. **33**, 1296–1308 (2007).

[16]J. M. G. Borsboom, C. T. Chin, and N. de Jong, "Nonlinear coded excitation method for ultrasound contrast imaging," Ultrasound Med. Biol. **29**, 277–284 (2003).

[17]Y. Sun, D. E. Kruse, and K. W. Ferrara, "Contrast imaging with chirped excitation," IEEE Trans. Ultrason. Ferroelectr. Freq. Control **54**, 520–529 (2007).

[18]J. Borsboom, C. T. Chin, and N. de Jong, "Experimental evaluation of a non-linear coded excitation method for contrast imaging," Ultrasonics **42**, 671–675 (2004).

[19]G. T. Clement, "Spectral image reconstruction for transcranial ultrasound measurement," Phys. Med. Biol. **50**, 5557–5572 (2005).

[20]G. Turin, "An introduction to matched filters," IRE Trans. Inf. Theory **6**, 311–329 (1960).

[21]P. C. Li, E. Ebbini, and M. O'Donnell, "A new filter design technique for coded excitation systems," IEEE Trans. Ultrason. Ferroelectr. Freq. Control **39**, 693–699 (1992).

[22]S. Triger, J. Saillant, C. E. M. Demore, S. Cochran, and D. R. S. Cumming, "Low-voltage coded excitation utilizing a miniaturized integrated ultrasound system employing piezoelectric 2-D arrays," IEEE Trans. Ultrason. Ferroelectr. Freq. Control **57**, 353–362 (2010).

[23]V. Behar and D. Adam, "Parameter optimization of pulse compression in ultrasound imaging systems with coded excitation," Ultrasonics **42**, 1101–1109 (2004).

[24]V. Behar and D. Adam, "Optimization of sparse synthetic transmit aperture imaging with coded excitation and frequency division," Ultrasonics **43**, 777–788 (2005).

[25]"Guidance for Industry and FDA Staff—Information for Manufacturers Seeking Marketing Clearance of Diagnostic Ultrasound Systems and Transducers," U.S. Department of Health and Human Services, 2008, pp. 31–32.

[26]P. C. Li, "Pulse compression for finite amplitude distortion based harmonic imaging using coded waveforms," Ultrason. Imaging **21**, 1–16 (1999).

[27]J. Song, S. Kim, H. Sohn, T. Song, and Y. M. Yoo, "Coded excitation for ultrasound tissue harmonic imaging," Ultrasonics **50**, 613–619 (2010).

[28]A. Nowicki, Z. Klimonda, M. Lewandowski, J. Litniewski, P. A. Lewin, and I. Trots, "Comparison of sound fields generated by different coded excitations–experimental results," Ultrasonics **44**, 121–129 (2006).

[29]M. F. Hamilton and D. T. Blackstock, *Nonlinear Acoustics* (Academic, New York, 1998), pp. 65–147.

[30]M. Abramowitz and I. A. Stegun, *Handbook of Mathematical Functions: With Formulas, Graphs, and Mathematical Tables* (Dover, New York, 1965).

[31]G. T. Clement, H. Nomura, and T. Kamakura, "A nonlinear bandwidth extension method for pulse compression," IEICE Technical Report No. 110, 2010, pp. 17–22